Biochemical Pharmacology 80 (2010) 50–61

Contents lists available at ScienceDirect

Biochemical Pharmacology

journal homepage: www.elsevier.com/locate/biochempharm

HMBA depolymerizes microtubules, activates mitotic checkpoints and induces mitotic block in MCF-7 cells by binding at the colchicine site in tubulin

Biswa Prasun Chatterji, Mithu Banerjee, Parminder Singh, Dulal Panda *

Department of Biosciences and Bioengineering, Indian Institute of Technology Bombay, Powai, Mumbai 400076, India

ARTICLE INFO

Article history:
Received 4 February 2010
Accepted 3 March 2010

Keywords:
Microtubule
HMBA
Apoptosis
Anticancer drugs
Spindle assembly checkpoint proteins
p53

ABSTRACT

10-[(3-Hydroxy-4-methoxybenzylidene)]-9(10H)-anthracenone (HMBA), a synthetic compound, has been reported to have a potent antitumor activity. In this study, we found that HMBA depolymerized microtubules in MCF-7 cells and produced aberrant spindles in the MCF-7 cells. It also reduced the distance between the centrosomes and activated the mitotic checkpoint proteins BubR1 and Mad2. Further, HMBA inhibited the progression of MCF-7 cells in mitosis and induced apoptotic cell death involving p53 pathway. *In vitro*, HMBA bound to purified brain tubulin with a dissociation constant of 4.1 ± 0.9 μM. It inhibited microtubule assembly and increased the GTP hydrolysis rate of microtubule assembly. The compound did not alter the binding of 2′(or 3′)-*O*-(trinitrophenyl) guanosine 5′-triphosphate (TNP–GTP), a fluorescent analogue of GTP, to tubulin suggesting that it did not inhibit the binding of GTP to tubulin. However, we obtained evidence indicating that HMBA perturbed the conformation of the GTP binding site in tubulin. In addition, an analysis of the modified Dixon plot suggested that HMBA competitively inhibited the binding of colchicine to tubulin. A computational analysis of the binding of HMBA to tubulin supported the finding that HMBA shared its binding site with colchicine in tubulin and indicated that the binding of HMBA to tubulin was primarily stabilized through hydrogen bonding.

1. Introduction

HMBA (Fig. 1) was used in several phase I and one phase II clinical trials against different human cancers in the 1980s and 1990s. It has shown solid tumor regression in several phase I trials when administered to patients with treatment-refractory or unresponsive tumors [1–3]. However, the efficacy was limited due to side-effects e.g. neurotoxicity or thrombocytopenia. In a phase II clinical trial involving patients suffering from myelodysplastic syndrome or acute myelogenous leukemia, HMBA caused a partial or complete amelioration of symptoms in 9 out of 41 patients [4]. Apart from anticancer activity, HMBA has also shown promise in treating HIV infections [5]. HMBA treatment of latent CD4+ T cells from recovering patients carrying HIV-1 showed clearance of the latent virus.

In spite of its relative success in clinical trials, its mode of action was not clear. Based upon studies on cultured cells, HMBA was thought to induce differentiation in malignant cells so that they return to normalcy after differentiation [6]. It was suggested that HMBA induced differentiation in murine erythroleukemia cells by modulating protein kinase C mediated signaling pathway and by suppressing cdk4-dependent kinase activity and hypophosphorylating retinoblastoma tumor suppressor protein [7,8]. HMBA has been suggested to inhibit Akt and MAPK signaling cascade in lung cancer cells [9]. Moreover HMBA has been shown to induce apoptosis in human myeloma cells, malignant pleural mesothelioma cells and hepatocellular carcinoma cells by down-regulating Bcl-2 [10–12]. A recent study has suggested that tubulin is the primary target of HMBA in cancer cells [13]. It was shown that HMBA inhibited the binding of colchicine to tubulin, prevented microtubule polymerization *in vitro* and in K562 (leukemia) cells and induced G2/M arrest in K562 and HeLa cells [13,14]. HMBA was also found to reduce the microtubule network and to increase the level of acetylated tubulin in a ciliated protozoa *Tetrahymena pyriformis* [15]. Further, sulfonate derivatives of HMBA were also found to inhibit the proliferation of HeLa, SF 268 and NCI-H460 cells in culture and to depolymerize microtubules *in vitro* [16].

Several inhibitors of microtubules are being successfully used in clinics for the treatment of different types of cancers [17,18]. These inhibitors have been found to stall cell proliferation and induce apoptotic cell death by diverse mechanisms; several of them have also been shown to suppress the dynamic instability of microtubules by directly interacting with tubulin [19,20]. Inhibitors of microtubule assembly have generally been found to bind to

Abbreviations: IgG, immunoglobulin G; GTP, guanosine triphosphate; GDP, guanosine diphosphate; FITC, fluorescein isothiocyanate; ANS, 1-anilinonaphthalene-8-sulfonic acid; EGTA, ethylene glycol-bis(β-aminoethyl ether)-N,N,N′,N′-tetraacetic acid; DAMA–colchicine, N-deacetyl-N-(2-mercaptoacetyl)-colchicine; PI, propidium Iodide; PBS, phosphate buffered saline; DMSO, dimethyl sulfoxide.

* Corresponding author. Tel.: +91 222576 7838/770; fax: +91 222572 3480.
E-mail address: panda@iitb.ac.in (D. Panda).

0006-2952/$ – see front matter © 2010 Elsevier Inc. All rights reserved.
doi:10.1016/j.bcp.2010.03.016

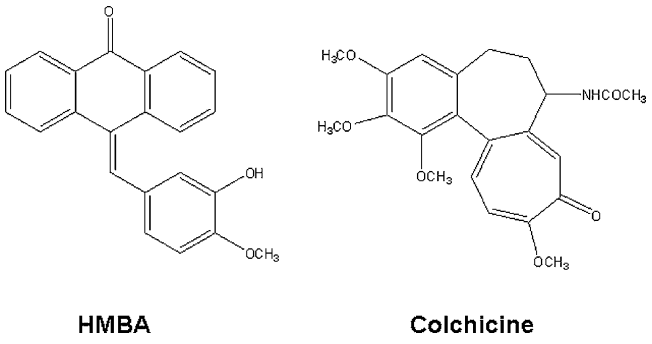

Fig. 1. Structures of HMBA and colchicine are shown.

tubulin in one of its two well-characterized sites, namely the vinblastine site or the colchicine binding site. However, the interaction of HMBA to tubulin, its binding site on tubulin and its antiproliferative mechanism of action are far from clear. In this study, we sought to unravel the mode of interaction of HMBA with tubulin and to determine the mechanism of antiproliferative action of HMBA using MCF-7 cells, a human breast cancer cell line.

Using both computational and experimental approaches, we have shown that HMBA binds to tubulin in the colchicine site and presented a mechanism through which it interacts with tubulin and inhibits microtubule polymerization. We have also provided significant insights into the mechanism through which HMBA activates mitotic checkpoint, inhibits mitosis and induces apoptosis in MCF-7 cells.

2. Materials and methods

2.1. Antibodies and compounds

Mouse monoclonal anti-α tubulin IgG, rabbit monoclonal γ-tubulin, FITC-labeled anti-rabbit IgG conjugate, bovine serum albumin (BSA), Hoechst 33258 were purchased from Sigma, MO, USA. Anti mouse IgG-Alexa 568 antibody and TNP–GTP were purchased from Molecular Probes, CA, USA. Mouse anti-p53, p21 antibodies and Annexin V-Propidium Iodide (PI) Apoptosis Detection Kit was purchased from Santa Cruz Biotechnology, CA, USA. Mouse anti-BubR1 and Mad2 antibodies were obtained from BD Biosciences, CA, USA. HMBA was purchased from Calbiochem, NJ, USA. Fetal bovine serum (FBS) was obtained from Biowest, Nuaille', France. All other reagents were of analytical grade and obtained from Sigma, MO, USA and Himedia, Mumbai, India.

2.2. Tubulin isolation

Microtubule proteins were isolated from goat brain by two cycles of assembly–disassembly process in the presence of 4 M glycerol, 5 mM $MgCl_2$, 1 mM EGTA and 0.5 mM GTP [21]. Pure tubulin (MAPs-free) was isolated from goat brains by two cycles of polymerization and depolymerization using 1 M monosodium glutamate buffer for assembly [22]. The composition of the assembly buffer was 1 M monosodium glutamate, 10% DMSO and 0.5 mM GTP. Depolymerization buffer contained 50 mM Pipes, pH 6.8, 1 mM EGTA, 3 mM $MgCl_2$ and 0.1 mM GTP. The protein was stored at −80 °C until further use. The protein concentration was determined by the method of Bradford using bovine serum albumin as standard [23].

2.3. Determination of the dissociation constant of tubulin and HMBA interaction

Tubulin (2 μM) in 25 mM Pipes, pH 6.8 was incubated in the absence and presence of different concentrations of HMBA (0.5–20 μM) for 30 min at 25 °C. The fluorescence emission spectra (310–360 nm) were monitored using 295 nm as the excitation wavelength. To minimize the inner filter effect, a cuvette of 0.3 cm path length was used. The inner filter effect was corrected using the formula:

$$F_{\text{corrected}} = F_{\text{observed}} \times \text{antilog}\left[\frac{A_{\text{ex}} + A_{\text{em}}}{2}\right]$$

where A_{ex} and A_{em} are the absorbance at the excitation and emission wavelengths and F_{observed} and $F_{\text{corrected}}$ are the observed and corrected fluorescence intensities, respectively. The dissociation constant (K_d) was calculated by fitting the fluorescence data in the following equation:

$$\Delta F = \frac{\Delta F_{\max} L}{K_d + L}$$

where ΔF and $\Delta F_{\max}$ represent change in the fluorescence intensity of the tubulin upon binding to HMBA and the maximum change in the fluorescence intensity of tubulin when it is fully bound with HMBA and L is the concentration of HMBA. ΔF was calculated by subtracting the fluorescence intensity of tubulin in the absence of HMBA from that in the presence of different concentrations of HMBA. The $\Delta F_{\max}$ was estimated using the Graph Pad Prism 5 software (Graph Pad Software, CA, USA).

2.4. Effect of HMBA on the fluorescence of tubulin–ANS complex

Tubulin (2 μM) in 25 mM Pipes buffer (pH 6.8) containing 1 mM EGTA, 3 mM $MgCl_2$ (PEM) was incubated in the absence and presence of different concentrations of HMBA at 25 °C for 10 min. Then, 20 or 260 μM ANS was added to the reaction mixtures and incubated for an additional 20 min. The fluorescence intensity was measured at 470 nm using 380 nm as the excitation wavelength. Experiment was repeated four times.

2.5. Competition between colchicine and HMBA for binding to tubulin

Tubulin (5 μM) was incubated without or with different concentrations of HMBA in PEM buffer in dark for 30 min at 25 °C. Then, colchicine (10 μM) was added to the reaction mixtures and incubated at 37 °C for an additional 1 h. Similarly, respective control solutions containing DMSO, colchicine (10 μM), HMBA (5, 10 and 25 μM) were incubated under identical conditions. The fluorescence spectrum of tubulin–colchicine complex was monitored using 340 nm as the excitation wavelength and the fluorescence intensity was noted at 430 nm.

2.6. Modified Dixon plot

Different concentrations of HMBA were mixed with tubulin along with a fixed concentration of colchicine. For one set, tubulin (5 μM) was mixed with different concentrations (0, 1, 2, 5, 10 and 15 μM) of HMBA and a fixed concentration of colchicine (5 μM) was added to the reaction mixtures. Similarly, two more sets were prepared with 15 and 20 μM colchicine. The mixtures were incubated at 37 °C for 1 h and the fluorescence of tubulin–colchicine complex was measured using 340 nm and 430 nm as excitation and emission wavelengths, respectively. The experiment was repeated thrice. $1/F$ (F = fluorescence intensity) versus HMBA concentration was plotted and inhibitory constant (K_i) was calculated using the modified Dixon plot [24,25].

2.7. Docking methodology

2.7.1. Preparation of receptor and the drug molecule

Similar to a previous study [26], we used tubulin–DAMA–colchicine crystal structure at 3.5 Å resolution (PDB CODE: 1SA01) as the reference structure. The coordinates for the ligands, bound GTP, GDP, and Mg^{2+} were removed from the crystal structure, all hydrogen atoms were added and the resultant structure was used as the receptor. The coordinates of the ligand, DAMA–colchicine, were retrieved from the crystal structure and the structure of colchicine was derived from the DAMA–colchicine coordinates by a minor modification of the side chain. The mol file for the HMBA structure was obtained from PRODRG server [27]. The structure of podophyllotoxin was also obtained from PRODRG [28].

2.7.2. Docking program and parameters used

We used LigandFit [29], a docking program within the Discovery Studio Version 2.1 (Accelrys, CA, USA) to find the putative binding site of HMBA on tubulin. The program uses a cavity detection algorithm, which explores the full range of infolded parts within a receptor as active site [30,31]. The docking simulation proceeds in two steps. The first step involves defining a binding site on the receptor. The second step uses a conformation shape-based docking. Several orientations of ligand are generated (Monte-Carlo algorithm) which are fitted into the cavities using a shape matching criteria. Flexible docking was simulated using Dreiding energy grid, with energy grid dielectric constant value of 1.0 and energy grid non-bonded cutoff distance of 10 Å. Thousand minimization iterations were carried out. The other parameters were: pose saving RMS threshold for diversity of 1.5, pose saving score threshold for diversity of 20.0, pose saving maximum clusters per molecule 5, pose saving RMS threshold for clustering 1.5 and docking RMS threshold for ligand/site match of 2.0 Å. In LigandFit the scoring is performed by employing several scoring functions which includes LigScore1, LigScore2, -PLP1, -PLP2, -PMF and DockScore. DockScore was used for scoring the results. It is a simple molecular mechanics force-field based scoring function which takes into account the summation of the ligand protein interaction energy and the internal energy of the ligand. Energy calculations involve the use of Dreiding force field. A total of 10 docking poses or docked structures were obtained. The pose having the highest score was used for the analysis of the putative interactions between the protein and the ligand.

2.8. CD spectroscopy

Tubulin (5 μM) was incubated without or with HMBA (25 μM) in 10 mM phosphate buffer for 30 min at 25 °C. The far-UV CD spectra (250–195 nm) were recorded using a 0.1 cm path length cuvette in a spectropolarimeter (Jasco J-810, Tokyo, Japan).

2.9. Light scattering

Tubulin (10 μM) in PEM buffer and 1 M monosodium glutamate (pH 6.8) was incubated without or with different concentrations (1–10 μM) of HMBA for 15 min on ice. Then, 1 mM GTP was added to the reaction mixtures. The assembly reaction was initiated by putting the reaction mixture in a cuvette at 37 °C. The assembly of microtubules was monitored by measuring light scattering intensity at 400 nm in a spectrofluorometer (Jasco FP-6500, Tokyo, Japan) at 37 °C. The assembly reached a steady state after 30 min. Light scattering intensity after 30 min of assembly was considered as the final level of polymer formed.

Similarly, MAPs-rich tubulin (1.2 mg/mL) was incubated without or with different concentrations of HMBA in 25 mM Pipes at pH 6.8 containing 5 mM $MgCl_2$ on ice for 15 min and then 1 mM GTP was added to this reaction mixture. The assembly kinetics was monitored as described previously.

2.10. Electron microscopy

Tubulin (10 μM) in PEM buffer was incubated with 1 M monosodium glutamate (pH 6.8) in the absence or presence of 5, 10, 25 μM HMBA on ice for 15 min and then, 1 mM GTP was added to the reaction mixture. The mixtures were polymerized for 25 min. Polymers were fixed with 0.5% glutaraldehyde and samples were prepared as described previously [32,33].

2.11. Tubulin GTPase assay

Tubulin (10 μM) in PEM buffer and 1 M monosodium glutamate was incubated in the absence or presence of different concentrations (5, 10, 25 and 50 μM) of HMBA on ice for 30 min. Then, 1 mM GTP was added to the reaction mixture and incubated at 37 °C. The amount of inorganic phosphate released after 30 min of hydrolysis was quantified by malachite green-ammonium molybdate assay [34,35]. Further, to check the effect of HMBA on the GTP hydrolysis rate of soluble tubulin under non-polymerizing condition, tubulin (10 μM) in PEM buffer was incubated in the absence or presence of different concentrations (5, 10, 25 and 50 μM) of HMBA on ice for 30 min. After incubation with 1 mM GTP for 30 min at 37 °C, inorganic phosphate release was estimated as described before [34,35]. Experiment was repeated three times.

2.12. TNP–GTP binding to tubulin

TNP–GTP has been used to probe GTP binding site in tubulin [36] and FtsZ [37]. Tubulin (3 μM) was mixed with different concentrations (0, 10, 25 and 50 μM) of HMBA in PEM buffer. TNP–GTP (20 μM) was added to each of the reaction mixture and incubated on ice for 4 h. Tubulin (3 μM) was incubated with GTP (1 mM) for 5 min and then with TNP–GTP (20 μM) on ice for 4 h. All the tubes were kept at 25 °C for 5 min before taking fluorescence reading in spectrofluorimeter (Jasco FP-6500, Tokyo, Japan). Excitation wavelength was 408 nm and emission range was 500–600 nm. Appropriate blank spectra were subtracted from the experimental spectra. This experiment was done twice.

2.13. Incorporation ratio of TNP–GTP to tubulin

Tubulin (20 μM) was incubated with TNP–GTP (100 μM) in presence of PEM buffer for 4 h on ice. This reaction mixture was loaded onto a Bio-Gel P6 resin (Bio-Rad, CA, USA) column in 1 cm × 15 cm glass column. The gel was swelled beforehand and equilibrated with PEM buffer. Flow rate of the column was kept at 0.5 mL per min and fractions collected were 500 μL each. Tubulin content of each fraction was measured by Bradford method [23] and TNP–GTP content was calculated by measuring absorbance at 408 nm ($\varepsilon_{408\ nm} = 2.3 \times 10^4\ M^{-1}\ cm^{-1}$) [36]. The incorporation of TNP–GTP per tubulin dimer in the absence and presence of HMBA was calculated by dividing bound TNP–GTP concentration by the protein concentration.

2.14. Cell culture

MCF-7 cells were grown in Minimal Essential Media (Himedia, Mumbai, India) supplemented with 10% (v/v) fetal bovine serum (FBS), 1% antibiotic–antimycotic solution (Himedia, Mumbai, India) containing streptomycin, amphotericin B, and penicillin, and sodium bicarbonate (2.2 g/L) at 37 °C in humidified chamber (Sanyo, Tokyo, Japan) with 5% CO_2 as described previously [38].

2.15. Effects of HMBA on the proliferation of MCF-7 cells

The half maximal proliferation inhibitory concentration (IC_{50}) of HMBA in MCF-7 cells was determined by counting the cells under a microscope as described previously [39]. Briefly, a 20 mM stock of HMBA was made in DMSO and the final concentration of DMSO in the culture media was kept less than 0.1% of the total volume of the media, 0.1% DMSO was used as a vehicle control for all experiments. MCF-7 cells (1×10^4 cells/well) were seeded in a polylysine coated 96-well tissue culture plate and grown for 24 h. MCF-7 cells were incubated with vehicle or different concentrations of HMBA for 48 h. Cells were detached from each well by trypsinization (0.025% trypsin and 1 mM EDTA in PBS) and live cells were counted manually by using a hemocytometer after staining with 0.4% trypan blue. The half maximal inhibition of cell proliferation (IC_{50}) was determined by plotting the percentage inhibition of cell proliferation against HMBA concentration. The experiment was performed thrice.

Percentage of mitotic cells in a population of MCF-7 cells treated without or with HMBA was determined by staining the chromosomes with Hoechst 33258 [40]. Briefly, MCF-7 cells (0.8×10^5 cells/mL) were grown on glass coverslips in a 24-well tissue culture plate for 24 h and then, incubated with vehicle or with different concentrations of HMBA (50,100 and 200 nM) for another 24 h. The cells were fixed with 3.7% formaldehyde, permeabilized with methanol at −20 °C and stained with Hoechst 33258 (1 μg/mL). The mitotic and interphase cells were counted under the Eclipse TE2000-U microscope (Nikon, Tokyo, Japan) using 40× objective. At least 600 cells were counted for each concentration of HMBA and the experiment was repeated three times.

2.16. Cell cycle analysis

MCF-7 cells were grown to confluency in 35 mm tissue culture dishes and the cells were then treated with vehicle or different concentrations of (100, 200 and 300 nM) HMBA for 24 h. The samples for FACS analysis was prepared as described previously [39]. Briefly, cell pellets were resuspended in 70% ethanol (ice-cold), centrifuged at $1000 \times g$ for 10 min and washed with PBS twice. Then, cells were suspended in 1 mL PBS, 50 μg/mL PI was added to the cell suspension along with RNaseA (200 μg/mL) and incubated on ice for 3 h before performing FACS analysis in a BD FACS Aria instrument (Becton Dickinson, CA, USA). DNA content of cells was measured by PI staining. Data were fit using Modfit LT version 3.2 (Verity Software House, ME, USA).

2.17. Immunofluorescence microscopy

Immunofluorescence microscopy for staining microtubules, centrosomes, p53, p21, BubR1 and Mad2 were performed as described previously [39,40,41]. Briefly, MCF-7 cells (0.8×10^5 cells/mL) were seeded on glass coverslips in 24-well plate. After 24 h of seeding, media were replaced with different concentrations of HMBA and incubated for another 24 h. The cells were fixed with 3.7% formaldehyde for half an hour at 37 °C and washed with PBS twice. Cells were permeabilized with methanol at −20 °C for 15 min and washed with PBS twice. To prevent non-specific binding of antibodies, coverslips were incubated with 2% BSA–PBS for 30 min at 37 °C. Then they were stained with primary antibody (1:300 dilution for α-tubulin, p53, p21 antibody; 1:500 for BubR1 and Mad2 antibody; 1:2000 for γ-tubulin antibody) for 2 h at 25 °C. The cells were washed with 2% BSA–PBS and incubated with secondary antibody (1:400 dilution for anti mouse Alexa-568 linked antibody in case of tubulin; 1:300 dilution for anti mouse Alexa-568 linked antibody in case of p53 and p21; 1:500 dilution for anti mouse Alexa-568 linked antibody in case of BubR1 and Mad2; 1:800 dilution for anti rabbit FITC linked antibody) for 1 h at 25 °C. Then cells were washed with PBS twice and incubated with Hoechst 33258 (1 μg/mL) for 10 min in dark to stain the DNA. After washing once with PBS, coverslips were mounted on clean glass slide with 80% glycerol in PBS containing 8 mg/mL DABCO (1,4-diazabicyclo [2.2.2] octane). The cover slips were observed under a Nikon Eclipse TE2000-U microscope using a 40× or 60× objective. The images were analyzed using Image-Pro Plus software (Media Cybernetics, MD, USA). The experiment was performed three times.

2.18. Apoptosis detection assay

2.18.1. Annexin V-PI staining

MCF-7 cells (0.8×10^5 cells/mL) were incubated in 24-well plate without or with different concentrations (50, 100 and 200 nM) of HMBA for 24 h [32]. We examined whether HMBA induced apoptosis in MCF-7 cells by visualizing HMBA treated cells after staining with Annexin V-FITC and PI as described in the manufacturer's protocol (Annexin V-PI Apoptosis Detection Kit, Santa Cruz Biotechnology, CA, USA).

3. Results

3.1. Interaction of HMBA with purified tubulin in vitro

HMBA reduced the intrinsic tryptophan fluorescence of tubulin in a concentration dependent manner indicating that the binding of HMBA induces a conformational change in tubulin (Fig. 2A). By fitting the fluorescence data in a binding isotherm, the dissociation constant of tubulin–HMBA interaction was determined to be 4.1 ± 0.9 μM at 25 °C (Fig. 2B).

HMBA also reduced the fluorescence of tubulin–ANS complex in a concentration dependent manner (Fig. 2C). For example, the fluorescence intensity of the tubulin–ANS complex was decreased by ∼30% and ∼67% in the presence of 2 and 8 μM HMBA, respectively. HMBA reduced the fluorescence of tubulin–ANS complex similarly in the presence of 20 and 260 μM ANS suggesting that HMBA did not inhibit the binding of ANS to tubulin and that the binding of HMBA to tubulin induced conformational change in the protein (Fig. 2D). However, HMBA did not alter the far-UV CD spectra of tubulin indicating that it does not perturb the secondary structure of tubulin (data not shown).

3.2. HMBA competitively inhibited the binding of colchicine to tubulin

HMBA inhibited the binding of radio-labeled colchicine to tubulin [13]; however, whether HMBA inhibited the binding of colchicine to tubulin in a competitive or noncompetitive manner was not known. We used the fluorescence of tubulin–colchicine complex to address the question. HMBA inhibited the formation of tubulin–colchicine complex in a concentration dependent manner supporting the previous finding that HMBA inhibits the colchicine binding to tubulin (Fig. 3A). Then, we analyzed the mode of inhibition of colchicine binding to tubulin by HMBA using the modified Dixon plot (Fig. 3B). The results suggested that HMBA inhibited colchicine binding to tubulin competitively and an inhibitor constant (K_i) of 3.6 ± 0.9 μM was determined from the plot.

3.3. Computational analysis of the binding of HMBA to tubulin

Several studies used tubulin–DAMA–colchicine crystal structure for simulating docking of different compounds at the colchicine binding site [42–45]. We used a commercial docking

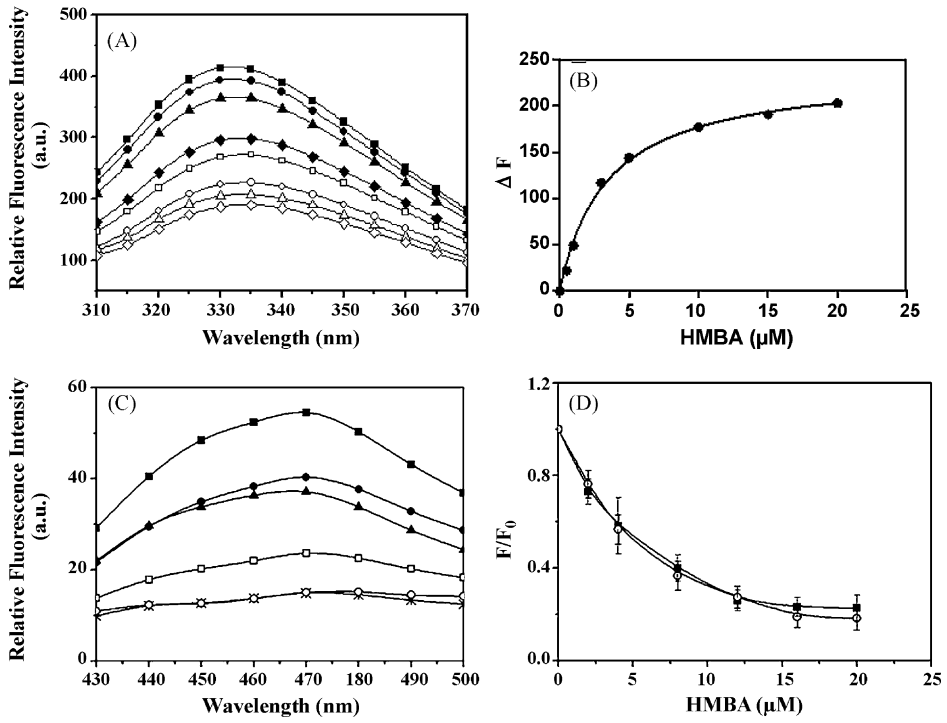

Fig. 2. Interaction of HMBA with tubulin monitored by fluorescence spectroscopy. Tubulin (2 μM) was incubated without or with a range of HMBA concentrations at 25 °C for 30 min in 25 mM Pipes, pH 6.8. (A) The fluorescence spectra of tubulin in the absence (■) and presence of 0.5 μM (●), 1 μM (▲), 3 μM (◆), 5 μM (□), 10 μM (○), 15 μM (Δ) and 20 μM (◇) of HMBA are shown. (B) Δ*F* (change in the fluorescence intensity of tubulin in arbitrary units) was plotted against HMBA concentrations. (C) Effect of different concentrations of HMBA on tubulin–ANS fluorescence. Tubulin (2 μM) was incubated in the absence (■) or presence of 1 μM (●), 4 μM (▲), 8 μM (□), 12 μM (○) and 25 μM (×) HMBA for 10 min at 25 °C. After 20 min incubation with ANS (20 μM) at 25 °C, the fluorescence of tubulin–ANS complex was recorded at 470 nm. (D) Effect of HMBA on tubulin–ANS fluorescence. Tubulin (2 μM) was incubated with different concentrations of HMBA and then, incubated with either 20 μM (■) or 260 μM (○) ANS. F_0 and F represent the fluorescence of tubulin–ANS complex in the absence and presence of different concentrations of HMBA, respectively. Average data with SD from 4 sets shown here.

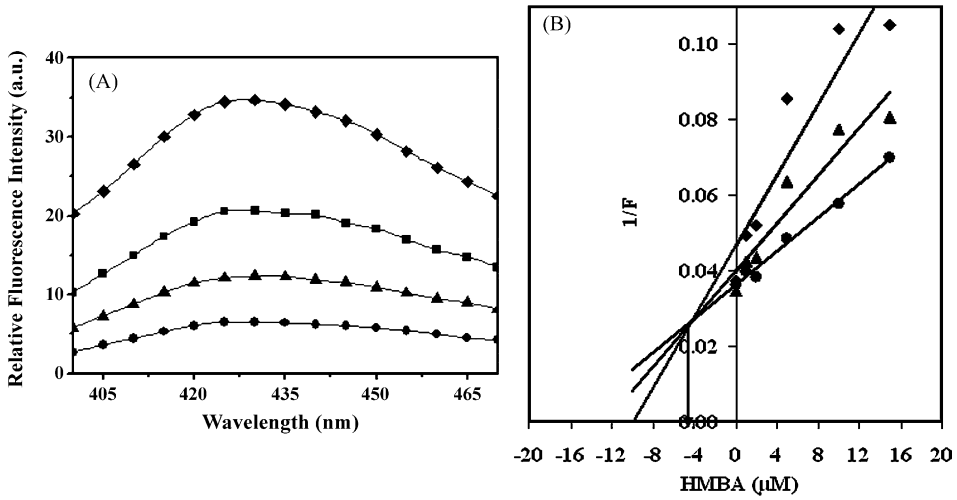

Fig. 3. HMBA competitively inhibited the binding of colchicine to tubulin. (A) HMBA reduced fluorescence of tubulin–colchicine complex. Tubulin (5 μM) was incubated in the absence (◆) or presence of 5 μM (■), 10 μM (▲), and 25 μM (●) of HMBA for 30 min at 25 °C. Then, the reaction mixtures were further incubated with colchicine (10 μM) at 37 °C for 1 h and tubulin–colchicine fluorescence was noted at 430 nm using 340 nm as the excitation wavelength. (B) Modified Dixon plot of the colchicine binding to tubulin in the presence of HMBA. Tubulin (5 μM) was incubated with HMBA (0–20 μM) and colchicine (5–20 μM) for 1 h at 37 °C. Then, tubulin–colchicine fluorescence at 430 nm was measured. Three different straight lines with 5 μM (◆), 15 μM (▲), 20 μM (●) of colchicine, respectively, intersected at a point beyond vertical axis. A perpendicular dropped from the point of intersection on the horizontal axis gives the value of K_i.

program LigandFit to dock HMBA in tubulin. Docking parameters were initially validated using tubulin–DAMA–colchicine crystal structure. The binding site was defined using a cavity-based method for detecting all probable binding sites within the receptor [29]. A total of 38 probable binding sites were elucidated on the receptor out of which the DAMA–colchicine binding cavity was selected because HMBA competitively inhibits colchicine binding to tubulin (Fig. 4B). DAMA–colchicine was docked at the predicted binding site of tubulin. A partition coefficient of five was used. The docked structure (shown in violet color in Fig. 4A) superimposed on the original crystal structure DAMA–colchicine–tubulin (shown in ash color in Fig. 4A). The RMS deviation for backbone

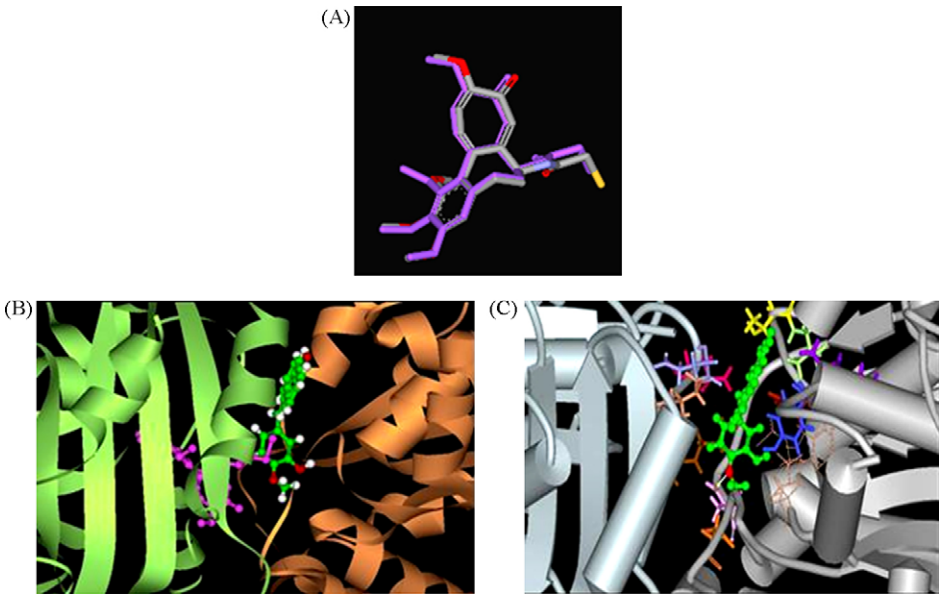

Fig. 4. Docking of HMBA on tubulin. (A) Docked DAMA–colchicine (violet) superimposed on DAMA–colchicine present in crystal structure (ash). The value of RMS deviation is 0.65 Å. (B) Sharing of binding region by colchicine (pink) and HMBA (green) in ball and stick model on tubulin represented in ribbon diagram. Beta chain (B-chain) is green and alpha chain (A-chain) is orange in color. (C) Receptor residues lying within 4 Å distance of docked HMBA (shown in stick model). The surrounding residues have been shown in different colors: The residues of the alpha chain (A-chain): GLN (A11) red; GLN (A15) violet; THR (A73) yellow; VAL (A74) green; ASN (A101) pink; ALA (A180) saffron; TYR (A224) blue. Residues of the beta-chain (B-chain): GLN (B247) violet; LEU (B248) orange; ASN (B249) magenta; LYS (B254) brown. The binding was favored by one hydrogen bond (white line) between the O34 oxygen atom of the aromatic methoxy substituent moiety of HMBA and the HD22 hydrogen atom of ASN (A101).

superimposition was 0.65 Å. Since a RMS deviation $\leq$2 Å indicates accurate docking [46], it could be inferred that the docking methodology used was appropriate. The binding sites of colchicine and podophyllotoxin, a competitive inhibitor of colchicine binding to tubulin, were also examined using this program. Both colchicine and podophyllotoxin exhibited high DockScore value of 80 and 75 suggesting that the DAMA–colchicine binding site as their binding site on tubulin (Table 1). Then, HMBA was docked into the active site of DAMA–colchicine using the same parameters. HMBA was found to dock well at the colchicine binding site (Fig. 4B). The active site residues lying within 4 Å distance of docked HMBA are portrayed in Fig. 4C and listed in Table 2. The O34 oxygen atom of the aromatic methoxy substituent moiety of HMBA formed a hydrogen bond to the HD22 hydrogen atom of the amino acid residue ASN-101 in the alpha chain (A-chain) of tubulin (Fig. 4C). The aromatic ring of TYR-224 could provide hydrophobic stabilization to HMBA. The residues encircling colchicine are given in Table 2. Both colchicine and HMBA binding site shared some common residues (shown in bold in Table 2).

Table 1
The dock score for different ligands.

Drug	Dock score
DAMA–colchicine	84
Colchicine	80
Podophyllotoxin	75
HMBA	62

Table 2
The residues lying within 4 Å distance of docked HMBA and colchicine in tubulin.

Drug	Residues
Colchicine	**ASN** (**A101**), SER (A178), THR (A179), **ALA** (**A180**), VAL (A181) VAL (B238), CYS (B241), LEU (B242), **LEU** (**B248**), ALA (B250), **LYS** (**B254**), LEU (B255), ASN (B258), MET (B259), THR (B314), VAL (B315), ALA (B316),VAL (B318), LYS (B352), ALA (B354), ILE (B378)
HMBA	GLN (A11), GLN (A15), THR (A73), VAL (A74), **ASN** (**A101**), **ALA** (**A180**), TYR (A224), GLN (B247), **LEU** (**B248**), ASN (B249), **LYS** (**B254**)

The common residues are shown in bold. The prefixes A and B to the residue numbers denote α and β chain of tubulin dimer.

3.4. HMBA depolymerized microtubules in vitro and caused aggregation

HMBA reduced the rate and extent of the light scattering intensity of the assembly of microtubule proteins suggesting that it inhibited microtubule assembly; 50% inhibition of the assembly occurred in the presence of 3.2 μM HMBA (Supplementary Fig. 1). In addition, HMBA inhibited the assembly of purified tubulin (MAPs-free) in a concentration dependent manner; 6.4 μM HMBA inhibited tubulin polymerization by 50% (Supplementary Fig. 1). As observed under electron microscope, tubulin polymerized with 1 M monosodium glutamate formed a network of microtubules. On incubation with 5 and 10 μM HMBA microtubules depolymerized and formed short pieces of protofilaments with fewer aggregates. At high concentrations of HMBA ($\geq$25 μM), large aggregates of tubulin were visible (Fig. 5).

3.5. HMBA increased GTP hydrolysis of tubulin under polymerizing conditions

Since HMBA inhibited tubulin polymerization, we examined its effect on the GTP hydrolysis rate of microtubules. Tubulin (10 μM) was polymerized without or with different concentrations of HMBA in the presence of 1 M monosodium glutamate and 1 mM GTP. HMBA increased the GTP hydrolysis rate (Fig. 6A). For example, 7.9 ± 2.9 and 16.9 ± 2.6 mole of inorganic phosphate/mole of tubulin were released in the absence or the presence 50 μM HMBA, respectively. However, HMBA did not significantly increase the GTP hydrolysis of soluble tubulin under non-polymerizing condition (in the absence of monosodium glutamate) suggesting that the increase in the GTP hydrolysis was not due to the increase of the hydrolysis by

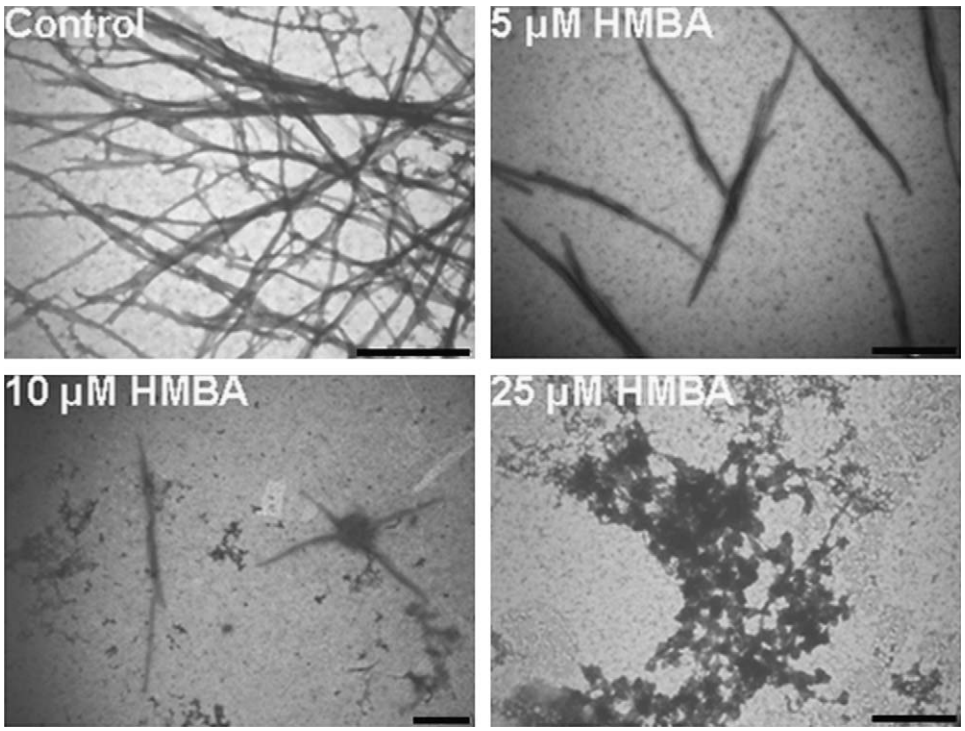

Fig. 5. Electron microscopic analysis of the assembly of the purified tubulin *in vitro*. Tubulin (10 μM) was polymerized in the presence of 1 M monosodium glutamate and 1 mM GTP without or with 5, 10, 25 μM HMBA. Scale bar 1 μm.

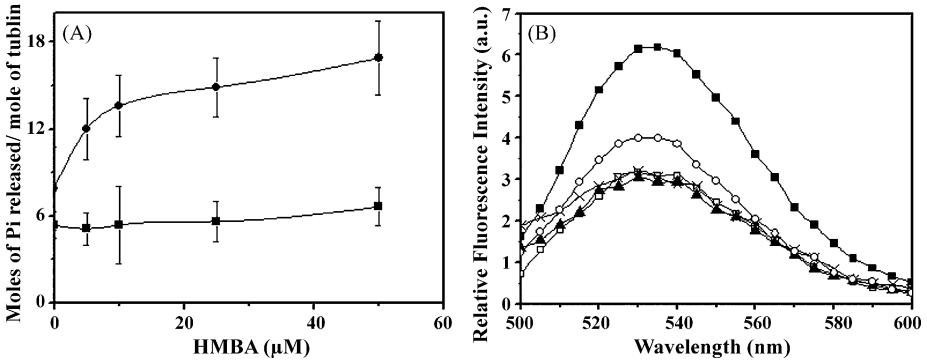

Fig. 6. Effects of HMBA on the hydrolysis and binding of GTP to tubulin. (A) Tubulin (10 μM) was incubated without or with (5, 10, 25, 50 μM) of HMBA and then, polymerized in the presence of 1 M monosodium glutamate and 1 mM GTP. The extent of GTP hydrolysis was measured after 30 min of assembly (●). Tubulin (10 μM) was incubated with 1 mM GTP without monosodium glutamate in absence or presence of HMBA (5, 10, 25, 50 μM) (■) and GTP hydrolysis was measured. Average of 3 sets of data with SD is shown. (B) Tubulin (3 μM) was incubated with TNP–GTP (20 μM) in the absence (■) or the presence of 10 μM (□), 25 μM (▲), 50 μM (×) HMBA and 1 mM GTP (○) for 4 h on ice. The emission spectra (500–600 nm) of TNP–GTP–tubulin were monitored by exciting at 408 nm.

soluble tubulin in the presence of HMBA (Fig. 6A). The increase in the hydrolysis could be due to a conformational change in the GTP binding site or due to the formation of small size polymers.

TNP–GTP, a fluorescent analog of GTP, has been shown to bind to the exchangeable GTP site in tubulin [36]. GTP (1 mM) reduced the fluorescence intensity of TNP–GTP–tubulin supporting the observation that TNP–GTP binds to tubulin in the GTP site. Incubation of tubulin with HMBA decreased TNP–GTP fluorescence suggesting that it induced conformational change in tubulin or inhibited the binding of TNP–GTP to tubulin (Fig. 6B).

To check whether the decrease in TNP–GTP fluorescence upon HMBA binding was due to a conformational change in the protein or due to the displacement of TNP–GTP from its binding site in tubulin by HMBA, the binding stoichiometry of TNP–GTP per tubulin dimer was determined by size-exclusion chromatography. The stoichiometry of TNP–GTP per tubulin dimer was calculated to be 0.50 ± 0.08 and 0.54 ± 0.05 in absence and presence of 50 μM HMBA, respectively indicating that HMBA did not displace TNP–GTP from its binding site in tubulin.

3.6. HMBA inhibited proliferation of MCF-7 cells by blocking the cell cycle progression in mitosis

HMBA inhibited MCF-7 proliferation in a concentration dependent fashion (Fig. 7A). For example, 10, 30 and 80 nM HMBA inhibited the proliferation by 7, 28 and 93%, respectively. The half maximal inhibition of proliferation (IC_{50}) was determined to be 47 ± 4 nM. HMBA-treatment caused a strong increase in the mitotic index of MCF-7 cells compared to that of the vehicle-treated cells. For example, $2.4 \pm 0.8\%$, $4.5 \pm 1.7\%$, $6.6 \pm 1.1\%$ and $24.4 \pm 3.9\%$ cells were in mitosis in the absence or the presence of 50, 100 and 200 nM HMBA, respectively.

The effect of HMBA on the cell cycle progression of MCF-7 was also examined by FACS analysis of the PI-stained cells (Fig. 7B).

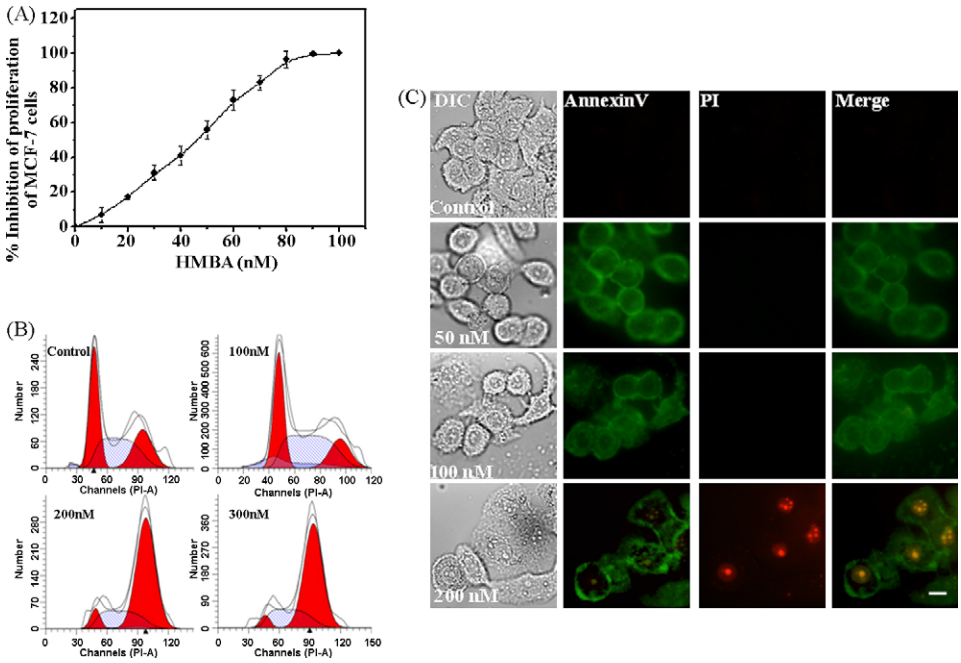

Fig. 7. HMBA inhibited the proliferation of MCF-7 cells, induced G2/M arrest and apoptosis in MCF-7 cells. MCF-7 cells were treated with different concentrations of HMBA for 24 or 48 h. (A) The effect of HMBA on cell proliferation was determined by counting cells as described in the experimental procedures. (B) Effects of HMBA on the cell cycle progression of MCF-7 cells were determined by FACS analysis. (C) HMBA induced apoptosis in MCF-7 cells. Annexin V-FITC (green) stains membrane whereas PI (red) stains nucleus. Apoptotic cells bear green membrane. Scale bar 10 μm. (For interpretation of the references to color in this figure legend, the reader is referred to the web version of the article.)

With HMBA treatment, greater numbers of cells were found to be accumulated in the G2/M phase. For example, 23% of the control cells (vehicle-treated cells) were found to be in the G2/M phase while 57 and 83% of the cells were found to be in the G2/M phase in the presence of 200 and 300 nM HMBA, respectively (Table 3).

3.7. HMBA induced apoptotic cell death

HMBA induced apoptosis in MCF-7 cells as ascertained by Annexin V/PI staining (Fig. 7C). In the presence of 50 and 100 nM HMBA, MCF-7 cells were found to be in early apoptosis phase

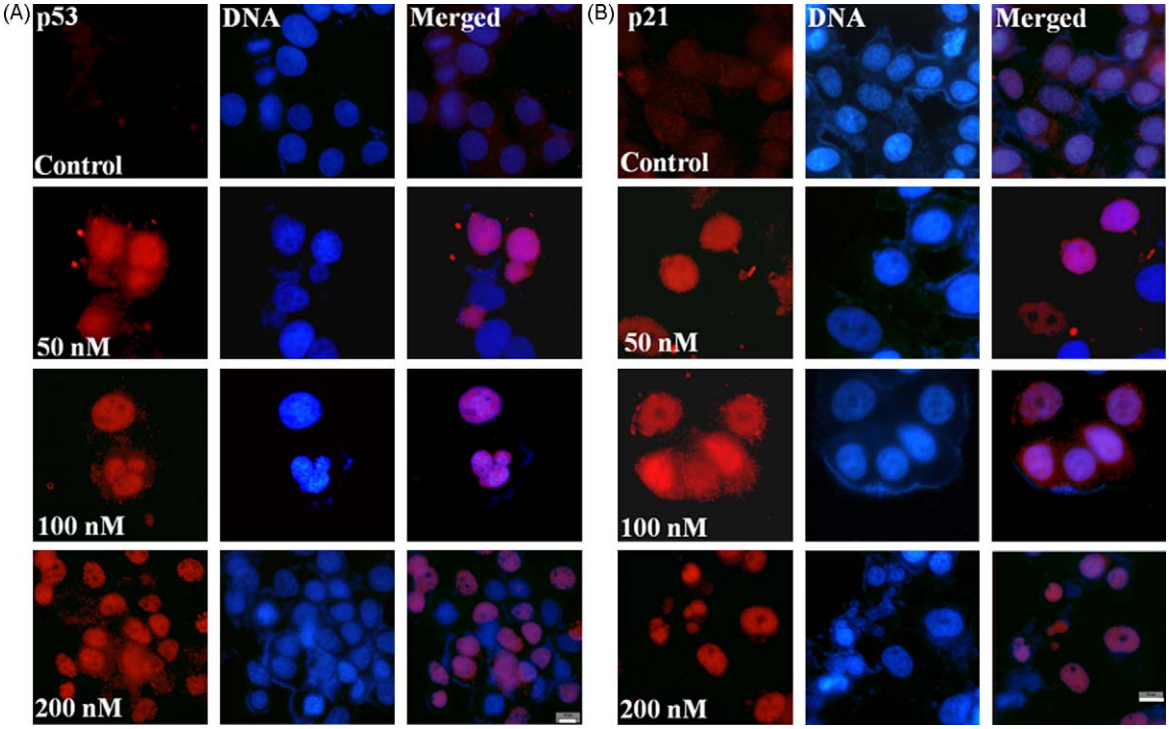

Fig. 8. HMBA treatment enhanced translocation of p53 and p21 into the nucleus. MCF-7 cells were treated without or with different concentrations of HMBA for 48 h. The nuclear localization of p53 and p21 was analyzed using antibody staining. (A) p53 (red), (B) p21 (red) and nucleus (blue) were stained as discussed in the materials and methods. Scale bar 10 μm. (For interpretation of the references to color in this figure legend, the reader is referred to the web version of the article.)

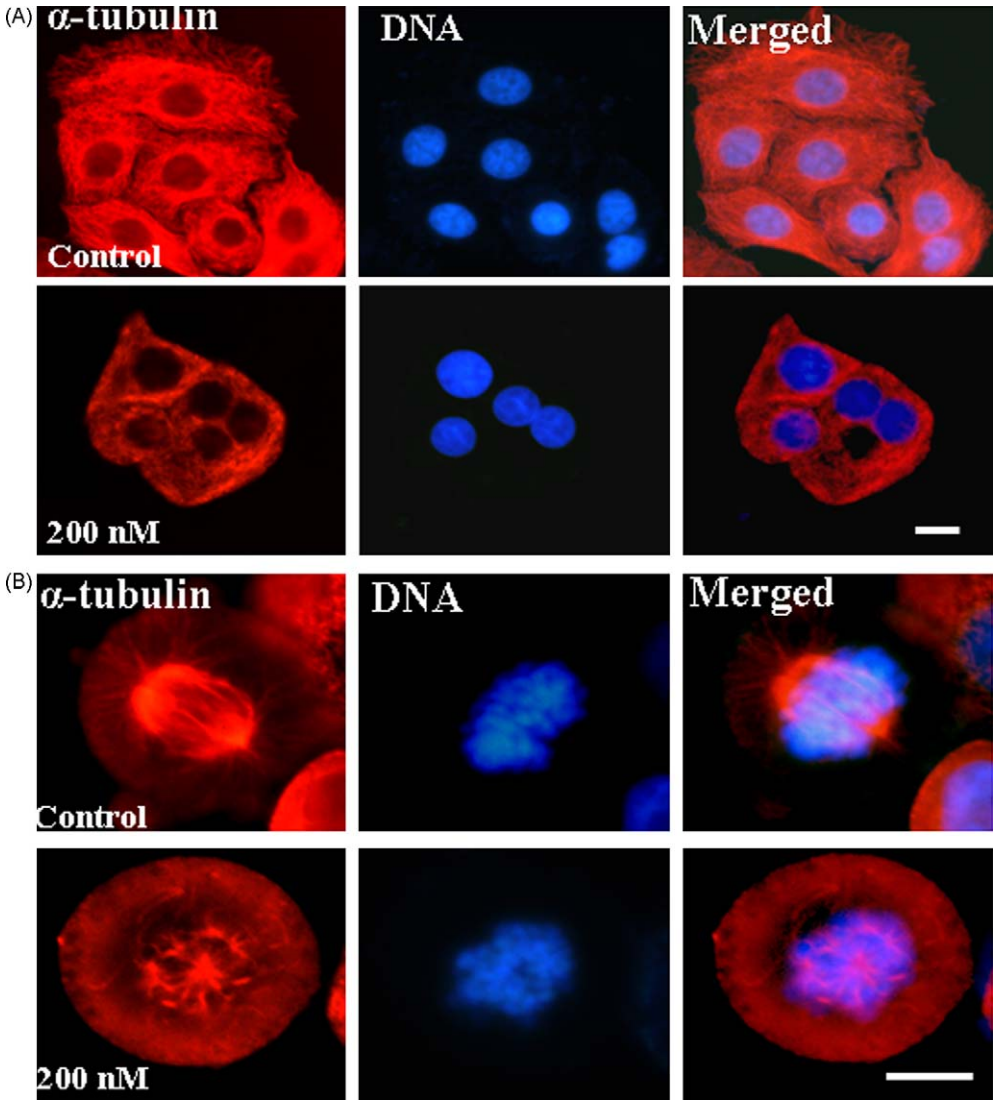

Fig. 9. HMBA perturbed microtubules and chromosome organizations. Effects of HMBA on the microtubules of interphase (A) and mitotic (B) MCF-7 cells are shown. Microtubules (red) and nucleus (blue) were stained as described in the materials and methods. Scale bar 10 μm. (For interpretation of the references to color in this figure legend, the reader is referred to the web version of the article.)

(green membrane but unstained nucleus) after 24 h; however, 200 nM HMBA induced cells into late apoptosis phase (Fig. 7C). HMBA treatment strongly increased the nuclear accumulation of p53 and p21 (Fig. 8A and B).

3.8. HMBA treatment depolymerized cellular microtubules and induced multipolarity in MCF-7 cells

HMBA-treatment caused depolymerization of microtubule network in MCF-7 cells (Fig. 9A and B). In the presence of 50 and 100 nM HMBA, the interphase microtubule network was not visibly altered while 200 nM HMBA strongly depolymerized the interphase microtubule network. Microtubule network was found to be thin and sparse in cell periphery when cells were treated with 200 nM HMBA (Fig. 9A).

In contrast to its modest effects on the interphase microtubules, low concentration (50 nM) of HMBA produced a strong effect on the spindle microtubules. In control MCF-7 cells, spindles were bipolar and chromosomes were condensed and arranged on the metaphase plates. HMBA exposure introduced aberrations in the spindles; for example, chromosomes were not organized on the metaphase plates (Fig. 9B). Further, it caused multipolar spindle formation. For example, $42.3 \pm 1.4\%$ and $70 \pm 0.3\%$ of the mitotic cells were found to be multipolar in the presence of 100 and 200 nM HMBA respectively. A significant fraction of the HMBA-treated cells was found to have multipolar spindles by gamma tubulin staining (Fig. 10). Chromosomes in multipolar cells looked like circular blob. They were not properly condensed and aligned as in control cells. The average distance between two poles in bipolar spindles of HMBA-treated cells were found to decrease as compared to the vehicle-treated control cells (Fig. 10). For example, in control cells, 9.3 ± 2.2 μm was the average distance between the poles and it decreased to 4.3 ± 1.6 μm upon 200 nM HMBA treatment (Fig. 10).

Table 3
Analysis of phases of cell cycle in MCF-7 cells after HMBA treatment.

Phase	Control (%)	100 nM (%)	200 nM (%)	300 nM (%)
G1	38	35	14	3
G2/M	23	18	57	83
S	39	47	29	14

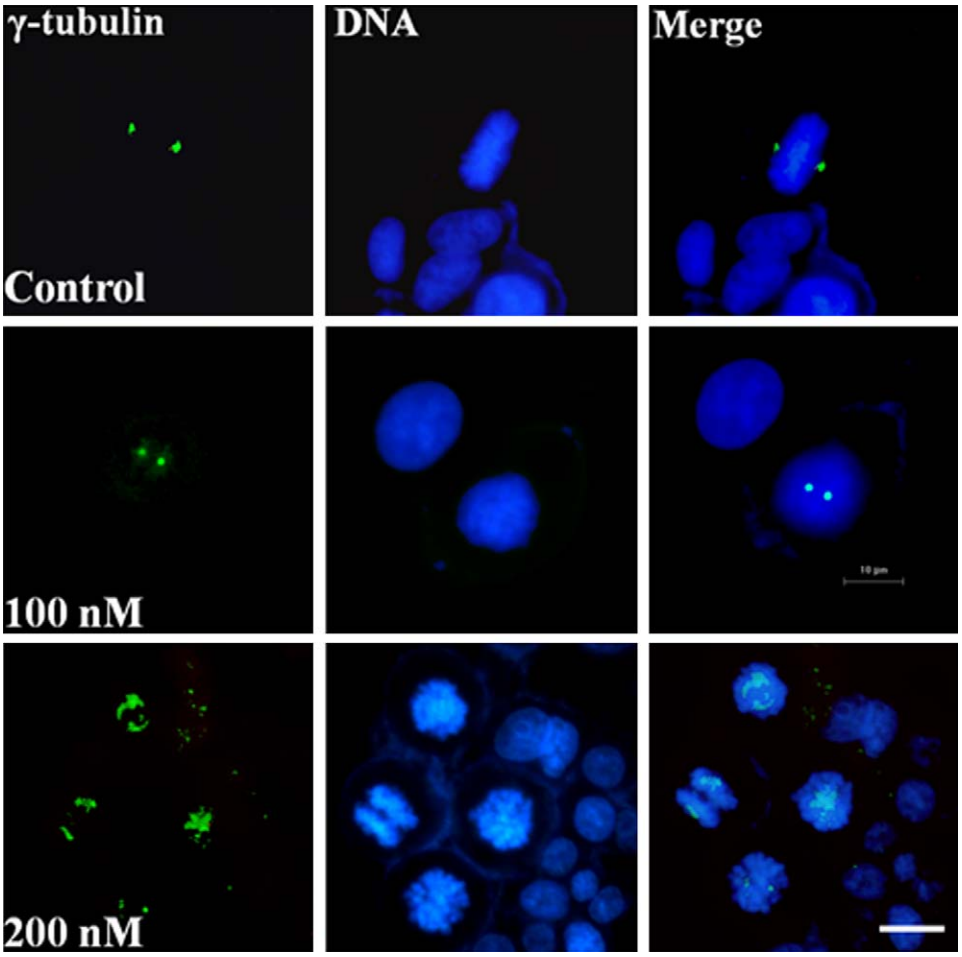

Fig. 10. Effect of HMBA on the organization of centrosomes. γ-tubulin (green) staining shows the location of centrosome (spindle pole) in mitotic MCF-7 cells. Nucleus (blue) was stained with Hoechst 33258 dye. Pole distances were calculated by Image Pro Plus software. Scale bar 10 μm. (For interpretation of the references to color in this figure legend, the reader is referred to the web version of the article.)

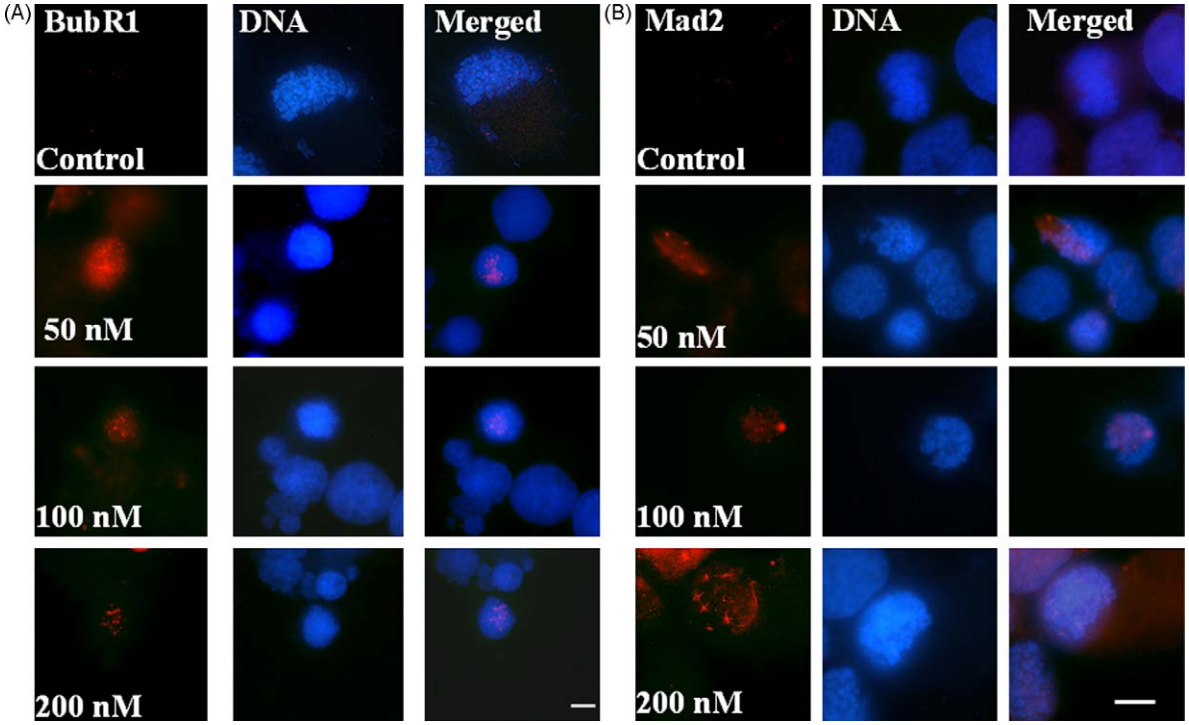

Fig. 11. HMBA treatment activated BubR1 (A) and Mad2 (B) in MCF-7 cells. BubR1 (red) and Mad2 (red) show localization over aberrantly organized chromosomes (blue). Scale bar 10 μm. (For interpretation of the references to color in this figure legend, the reader is referred to the web version of the article.)

3.9. HMBA activated spindle assembly checkpoint

As expected mitotic checkpoint proteins, BubR1 and Mad2, were not seen in the vehicle treated control mitotic cells (Fig. 11). These proteins were observed in the MCF-7 cells treated with 50, 100 and 200 nM of HMBA. In the HMBA-treated mitotic cells, chromosomes were not properly condensed and found to be misaligned. BubR1 and Mad2 were found to be colocalized over these uncondensed chromosomes indicating the activation of the checkpoint proteins in HMBA-treated cells (Fig. 11).

4. Discussion

HMBA depolymerized microtubules in MCF-7 cells, damaged the mitotic spindles, reduced pole-to-pole distance in bipolar spindles, activated mitotic checkpoint proteins, stalled the cells at mitosis and induced multipolarity in MCF-7 cells. Shortened bipolar spindle and misaligned chromosomes in HMBA-treated cells imply a loose microtubule–kinetochore attachment in these cells. Further, HMBA was found to bind to tubulin with a dissociation constant of 4.1 ± 0.9 μM indicating that it binds to tubulin strongly when compared with several known microtubule depolymerizing agents such as noscapine, vinblastine, estramustine and griseofulvin. Noscapine [47], vinblastine [48], estramustine [49], and griseofulvin [50], are having low affinity towards tubulin with K_d of 144, 43, 30 and 300 μM, respectively. However, HMBA binds to tubulin weakly as compared to colchicine [51].

HMBA reduced the development of colchicine–tubulin fluorescence indicating that it may bind to the colchicine binding site in tubulin. Further, an analysis of the modified Dixon plot suggested that HMBA competitively inhibits colchicine binding to tubulin with a K_i value of 3.6 ± 0.9 μM. Although HMBA has no structural resemblance to colchicine, it docked preferentially at the same site. Both drugs shared four common residues ASN (A101), ALA (A180), LEU (B248), and LYS (B254) at the binding region. However, HMBA binding was favored by hydrogen bonding whereas colchicine showed no such hydrogen bond formation. Moreover, HMBA was encircled by aromatic as well as aliphatic non-polar and polar residues, whereas only several aliphatic non-polar and polar residues surrounded colchicine. The hydrophobic anthracenone moiety of HMBA may prefer a more hydrophobic environment relative to colchicine, which lacks such a hydrophobic moiety. Though HMBA docked at the colchicine site in tubulin, the mode of interaction with surrounding residues was not similar to that of colchicine. For example, HMBA does not change the secondary structure of tubulin whereas colchicine is known to perturb the secondary structure of tubulin [52].

HMBA reduced the tryptophan fluorescence of tubulin indicating that it induced conformational change in tubulin. HMBA competitively inhibited the binding of colchicine to tubulin and the docking analysis also suggested that it binds to colchicine site in tubulin. ANS and colchicine are known to have distinct binding sites in tubulin [53]; therefore, HMBA binds to tubulin at a site, which is different from the ANS site. HMBA reduced the tubulin–ANS fluorescence indicating that either it inhibited the binding of ANS to tubulin or induced conformational change in tubulin. The changes in fluorescence intensity of tubulin–ANS complex incubated with two different concentrations (20 or 260 μM) of ANS were found to be similar in the presence of different concentrations of HMBA (Fig. 2D). The result indicated that the reduction in the fluorescence intensity of tubulin–ANS complex in the presence of HMBA was due to a conformational change in tubulin rather than the inhibition of ANS binding to tubulin.

HMBA increased the GTP hydrolysis of microtubule assembly in the presence of 1 M monosodium glutamate. However, unlike colchicine it did not increase the GTPase activity of the soluble tubulin. We reasoned that the stimulation of the GTPase activity of tubulin by HMBA in polymerizing conditions could be due to the HMBA-induced conformational change in the GTP binding site of tubulin. In support of this idea, HMBA was found to decrease the fluorescence of tubulin–TNP–GTP complex. HMBA did not reduce the binding of TNP–GTP to tubulin as the incorporation stoichiometry of TNP–GTP per tubulin dimer remained constant in the presence or absence of HMBA. HMBA may increase the GTP hydrolysis rate of microtubules by inducing conformational change in tubulin, which in turn causes depolymerization of microtubules.

We found an increase in the GTP hydrolysis rate despite the depolymerization of microtubules with increasing concentrations of HMBA. This could be due to the formation of multiple oligomers of tubulin or short polymers of tubulin. Electron microscopic analysis suggested the formation of short polymers with 5 μM HMBA concentration. With 10 μM HMBA concentration, there were short polymers as well as aggregates whereas with 25 μM HMBA, large size aggregates were seen. Dynamic light scattering measurements also suggested that HMBA induces aggregation of tubulin dimers in the presence of 1 M monosodium glutamate (data not shown).

HMBA inhibited MCF-7 proliferation with an IC_{50} of 47 ± 4 nM. HMBA, at its half-maximal proliferation inhibitory concentration range, did not cause a marked depolymerization of microtubules as evident from α-tubulin staining. HMBA-treatment activated p53 and its downstream protein p21 and caused their nuclear accumulation and induced apoptosis. It can be suggested that similar to several other tubulin targeting agents such as vinblastine, colchicine [54], benomyl [40] and estramustine [39], HMBA also suppresses microtubule dynamics and that the stabilization of microtubule dynamics by HMBA may initiate p53 translocation to the nucleus. HMBA also activated spindle assembly checkpoint proteins BubR1 and Mad2, which signify improper kinetochore–microtubule attachment due to the perturbation of microtubule assembly dynamics. Reduced spindle pole distance as observed by γ-tubulin staining in HMBA treated cells suggests loose kinetochore–microtubule attachment. Noscapine and Benomyl disturb kinetochore–microtubule attachment and activate mitotic checkpoints by attenuating dynamic microtubules [55,41].

In summary, HMBA was found to increase the GTP hydrolysis rate and to depolymerize microtubules by interacting with tubulin at the colchicine site. It activated mitotic checkpoint in MCF-7 cells, inhibited mitosis in these cells and induced p53-mediated apoptotic cell death.

Acknowledgements

This work is supported by a grant from the Council of Scientific and Industrial Research, Government of India to DP. DP is a Swarnajayanti fellow. We thank Centre for Research in Nanotechnology and Science of Indian Institute of Technology Bombay for FACS facility. We thank Sonia Kapoor and Bhavya Jindal for critically reading the manuscript.

Appendix A. Supplementary data

Supplementary data associated with this article can be found, in the online version, at doi:10.1016/j.bcp.2010.03.016.

References

[1] Young CW, Fanucchi MP, Declan Walsh T, Baltzer L, Yaldaei S, Stevens YW, et al. Phase I trial and clinical pharmacological evaluation of hexamethylene bisacetamide administration by ten-day continuous intravenous infusion at twenty-eight-day intervals. Cancer Res 1988;48:7304–9.

[2] Conley BA, Forrest A, Egorin MJ, Zuhowski EG, Sinibaldi V, Van Echo DA. Phase I trial using adaptive control dosing of hexamethylene bisacetamide (NSC 95580). Cancer Res 1989;49:3436–40.
[3] Egorin MJ, Sigman LM, VanEcho DA, Forrest A, Whitacre MY, Aisner J. Phase I clinical and pharmacokinetic study of hexamethylene bisacetamide (NSC 95580) administered as a five-day continuous infusion. Cancer Res 1987; 47:617–23.
[4] Andreeff M, Stone R, Michaeli J, Young CW, Tong WP, Sogoloff H, et al. Hexamethylene bisacetamide in myelodysplastic syndrome and acute myelogenous leukemia: a phase II clinical trial with a differentiation-inducing agent. Blood 1992;80:2604–9.
[5] Choudhary SK, Archin NM, Margolis DM. Hexamethylene bisacetamide and disruption of human immunodeficiency virus type 1 latency in CD4 (+) T cells. J Infect Dis 2008;197:1162–70.
[6] Marks PA, Richon VM, Kiyokawa H, Rifkind RA. Inducing differentiation of transformed cells with hybrid polar compounds: a cell cycle-dependent process. Proc Natl Acad Sci USA 1994;91:10251–4.
[7] Kiyokawa H, Richon VM, Rifkind RA, Marks PA. Suppression of cyclin-dependent kinase 4 during induced differentiation of erythroleukemia cells. Mol Cell Biol 1994;14:7195–203.
[8] Leng L, Yu F, Dong L, Busquets X, Osada S, Richon VM, et al. Differential modulation of protein kinase C isoforms in erythroleukemia during induced differentiation. Cancer Res 1993;53:5554–8.
[9] Dey A, Wong E, Kua N, Teo HL, Tergaonkar V, Lane D. Hexamethylene bisacetamide (HMBA) simultaneously targets AKT and MAPK pathway and represses NF κβ activity: implications for cancer therapy. Cell Cycle 2008; 7:3759–67.
[10] Siegel DS, Zhang X, Feinman R, Teitz T, Zelenetz A, Richon VM, et al. Hexamethylene bisacetamide induces programmed cell death (apoptosis) and downregulates Bcl-2 expression in human myeloma cells. Proc Natl Acad Sci USA 1998;95:162–6.
[11] Palumbo C, Albonici L, Bei R, Bocci C, Scarpa S, Di Nardo P, et al. HMBA induces cell death and potentiates doxorubicin toxicity in malignant mesothelioma cells. Cancer Chemother Pharmacol 2004;54:398–406.
[12] Ouyang GL, Cai QF, Liu M, Chen RC, Huang Z, Jiang RS, et al. Growth arrest and apoptosis of human hepatocellular carcinoma cells induced by hexamethylene bisacetamide. World J Gastroenterol 2004;10:954–8.
[13] Prinz H, Ishii Y, Hirano T, Stoiber T, Camacho Gomez JA, Schmidt P, et al. Novel benzylidene-9(10H)-anthracenones as highly active antimicrotubule agents. Synthesis, antiproliferative activity, and inhibition of tubulin polymerisation. J Med Chem 2003;46:3382–94.
[14] Zuse A, Schmidt P, Baasner S, Böhm KJ, Müller K, Gerlach M, et al. Sulfonate derivatives of naphtho[2,3-b]thiophen-4(9H)-one and 9(10H)-anthracenone as highly active antimicrotubule agents. Synthesis, antiproliferative activity, and inhibition of tubulin polymerisation. J Med Chem 2007;50:6059–66.
[15] Kovács P, Pállinger E, Csaba G. Effect of hexamethylene bisacetamide (HMBA) on the microtubular system of *Tetrahymena pyriformis*. Comp Biochem Physiol B Biochem Mol Biol 2008;149:259–64.
[16] Zuse A, Prinz H, Müller K, Schmidt P, Günther EG, Schweizer F, et al. 9-Benzylidene-naphtho[2,3-b]thiophen-4-ones and benzylidene-9(10H)-anthracenones as novel tubulin interacting agents with high apoptosis-inducing activity. Eur J Pharmacol 2007;575:34–45.
[17] Perez EA. Microtubule inhibitors: differentiating tubulin-inhibiting agents based on mechanisms of action, clinical activity, and resistance. Mol Cancer Ther 2009;8:2086–95.
[18] Carlson RO. New tubulin targeting agents currently in clinical development. Exp Opin Investig Drugs 2008;17:707–22.
[19] Singh P, Rathinasamy K, Mohan R, Panda D. Microtubule assembly dynamics: an attractive target for anticancer drugs. IUBMB Life 2008;60:368–75.
[20] Jordan MA, Wilson L. Microtubules as a target for anticancer drugs. Nat Rev Cancer 2004;4:253–65.
[21] Shelanski ML, Gaskin F, Cantor CR. Microtubule assembly in the absence of added nucleotides. Proc Natl Acad Sci USA 1973;70:765–8.
[22] Hamel E, Lin CM. Glutamate-induced polymerization of tubulin: characteristics of the reaction and application to the large-scale purification of tubulin. Arch Biochem Biophys 1981;209:29–40.
[23] Bradford MM. A rapid and sensitive method for the quantitation of microgram quantities of protein utilizing the principle of protein–dye binding. Anal Biochem 1976;72:248–54.
[24] Dixon M. The determination of enzyme inhibitor constants. Biochem J 1952;55:170–1.
[25] Acharya BR, Bhattacharyya B, Chakrabarti G. The natural naphthoquinone plumbagin exhibits antiproliferative activity and disrupts the microtubule network through tubulin binding. Biochemistry 2008;47:7838–45.
[26] Ravelli RB, Gigant B, Curmi PA, Jourdain I, Lachkar S, Sobel A, et al. Insight into tubulin regulation from a complex with colchicine and a stathmin-like domain. Nature 2004;428:198–202.
[27] Schüttelkopf AW, van Aalten DM. PRODRG: a tool for high-throughput crystallography of protein–ligand complexes. Acta Crystallogr D Biol Crystallogr 2004;60:1355–63.
[28] van Aalten DM, Bywater R, Findlay JB, Hendlich M, Hooft RW, Vriend G. PRODRG, a program for generating molecular topologies and unique molecular descriptors from coordinates of small molecules. J Comput Aided Mol Des 1996;10:255–62.
[29] Venkatachalam CM, Jiang X, Oldfield T, Waldman M. LigandFit: a novel method for the shape-directed rapid docking of ligands to protein active sites. J Mol Graph Model 2003;21:289–307.
[30] Montes M, Miteva MA, Villoutreix BO. Structure-based virtual ligand screening with LigandFit: pose prediction and enrichment of compound collections. Proteins 2007;68:712–25.
[31] Montes M, Braud E, Miteva MA, Goddard ML, Mondésert O, Kolb S, et al. Receptor-based virtual ligand screening for the identification of novel CDC25 phosphatase inhibitors. J Chem Inf Model 2008;48:157–65.
[32] Srivastava P, Panda D. Rotenone inhibits mammalian cell proliferation by inhibiting microtubule assembly through tubulin binding. FEBS J 2006;274: 4788–801.
[33] Gupta KK, Bharne SS, Rathinasamy K, Naik NR, Panda D. Dietary antioxidant curcumin inhibits microtubule assembly through tubulin binding. FEBS J 2006;273:5320–32.
[34] Baykov AA, Evtushenko OA, Avaeva SM. A malachite green procedure for orthophosphate determination and its use in alkaline phosphatase-based enzyme immunoassay. Anal Biochem 1988;171:266–70.
[35] Gupta K, Panda D. Perturbation of microtubule polymerization by quercetin through tubulin binding: a novel mechanism of its antiproliferative activity. Biochemistry 2002;41:13029–38.
[36] Han Y, Malak H, Chaudhary AG, Chordia MD, Kingston DG, Bane S. Distances between the paclitaxel, colchicine and exchangeable GTP binding sites on tubulin. Biochemistry 1998;37:6636–44.
[37] Jaiswal R, Beuria TK, Mohan R, Mahajan SK, Panda D. Totarol inhibits bacterial cytokinesis by perturbing the assembly dynamics of FtsZ. Biochemistry 2007;46:4211–20.
[38] Clément MJ, Rathinasamy K, Adjadj E, Toma F, Curmi PA, Panda D. Benomyl and colchicine synergistically inhibit cell proliferation and mitosis: evidence of distinct binding sites for these agents in tubulin. Biochemistry 2008;47:13016–25.
[39] Mohan R, Panda D. Kinetic stabilization of microtubule dynamics by estramustine is associated with tubulin acetylation, spindle abnormalities, and mitotic arrest. Cancer Res 2008;68:6181–9.
[40] Rathinasamy K, Panda D. Kinetic stabilization of microtubule dynamic instability by benomyl increases the nuclear transport of p53. Biochem Pharmacol 2008;76:1669–80.
[41] Rathinasamy K, Panda D. Suppression of microtubule dynamics by benomyl decreases tension across kinetochore pairs and induces apoptosis in cancer cells. FEBS J 2006;273:4114–28.
[42] Chiang YK, Kuo CC, Wu YS, Chen CT, Coumar MS, Wu JS, et al. Generation of ligand-based pharmacophore model and virtual screening for identification of novel tubulin inhibitors with potent anticancer activity. J Med Chem 2009; 52:4221–33.
[43] Romagnoli R, Baraldi PG, Carrion MD, Cara CL, Cruz-Lopez O, Tolomeo M, et al. Design, synthesis and structure-activity relationship of 2-(3′,4′,5′-trimethoxybenzoyl)-benzo[b]furan derivatives as a novel class of inhibitors of tubulin polymerisation. Bioorg Med Chem 2009;17:6862–71.
[44] Putey A, Popowycz F, Do QT, Bernard P, Talapatra SK, Kozielski F, et al. Indolobenzazepin-7-ones and 6-, 8-, and 9-membered ring derivatives as tubulin polymerization inhibitors: synthesis and structure–activity relationship studies. J Med Chem 2009;52:5916–25.
[45] Alvarez R, Alvarez C, Mollinedo F, Sierra BG, Medarde M, Peláez R. Isocombretastatins A: 1,1-diarylethenes as potent inhibitors of tubulin polymerization and cytotoxic compounds. Bioorg Med Chem 2009;17:6422–31.
[46] Wang R, Lu Y, Wang S. Comparative evaluation of 11 scoring functions for molecular docking. J Med Chem 2003;46:2287–303.
[47] Aneja R, Vangapandu SN, Lopus M, Viswesarappa VG, Dhiman N, Verma A, et al. Synthesis of microtubule-interfering halogenated noscapine analogs that perturb mitosis in cancer cells followed by cell death. Biochem Pharmacol 2006;72:415–26.
[48] Lee JC, Harrison D, Timasheff SN. Interaction of vinblastine with calf brain microtubule protein. J Biol Chem 1975;250:9276–82.
[49] Panda D, Miller HP, Islam K, Wilson L. Stabilization of microtubule dynamics by estramustine by binding to a novel site in tubulin: a possible mechanistic basis for its antitumor action. Proc Natl Acad Sci USA 1997;94:10560–4.
[50] Panda D, Rathinasamy K, Santra MK, Wilson L. Kinetic suppression of microtubule dynamic instability by griseofulvin: implications for its possible use in the treatment of cancer. Proc Natl Acad Sci USA 2005;102:9878–83.
[51] Panda D, Roy S, Bhattacharyya B. Reversible dimer dissociation of tubulin S and tubulin detected by fluorescence anisotropy. Biochemistry 1992;31:9709–16.
[52] Detrich III HW, Williams Jr RC, Macdonald TL, Wilson L, Puett D. Changes in the circular dichroic spectrum of colchicine associated with its binding to tubulin. Biochemistry 1981;20:5999–6005.
[53] Ward LD, Timasheff SN. Energy transfer studies of the distance between the high-affinity metal binding site and colchicine and 8-anilino1-napthalenesulfonic acid binding sites on tubulin. Biochemistry 1988;27:1508–14.
[54] Giannakakou P, Nakano M, Nicolaou KC, O'Brate A, Yu J, Blagosklonny MV, et al. Enhanced microtubule-dependent trafficking and p53 nuclear accumulation by suppression of microtubule dynamics. Proc Natl Acad Sci USA 2002;99: 10855–60.
[55] Zhou J, Panda D, Landen JW, Wilson L, Joshi HC. Minor alteration of microtubule dynamics causes loss of tension across kinetochore pairs and activates the spindle checkpoint. J Biol Chem 2002;277:17200–8.